Entrainment of Micromechanical Limit Cycle Oscillators in the Presence of Frequency Instability

David B. Blocher, Alan T. Zehnder, and Richard H. Rand

***Abstract*—The nonlinear dynamics of micromechanical oscillators are explored experimentally. Devices consist of singly and doubly supported Si beams, 200 nm thick and 35 μm long. When illuminated within a laser interference field, devices self-oscillate in their first bending mode due to feedback between laser heating and device displacement. Compressive prestress buckles doubly supported beams leading to a strong amplitude–frequency relationship. Significant frequency instability is seen in doubly supported devices. Self-resonant beams are also driven inertially with varying drive amplitude and frequency. Regions of primary, sub-, and superharmonic entrainment are measured. Statistics of primary entrainment are measured for low drive amplitudes, where the effects of frequency instability are measurable. Sub- and superharmonic entrainment are not seen in singly supported beams. A simple model is built to explain why high-order entrainment is seen only in doubly supported beams. Its analysis suggests that the strong amplitude–frequency relationship in doubly supported beams enables hysteresis, wide regions of primary entrainment, and high orders of sub- and superharmonic entrainment. [2012-0225]**

***Index Terms*—Limit cycles, micromechanical devices, optical resonators, oscillators, thermomechanical processes.**

I. Introduction

In RESONANT sensing applications, the frequency of oscillation of a microelectromechanical systems (MEMS) device carries information about the quantity of interest. Devices have been built to transduce a number of quantities that interact with their frequency, such as temperature [1], pressure [2], [3], or bound-mass [4]–[7]. To obtain periodic motion, devices may be driven electrostatically [8], piezoelectrically [9], magnetically [10], or thermo-optically [11]–[14] using an externally modulated drive. Such designs require an external highly stable frequency source. Resonant MEMS have also been fabricated within active-electrical [15], active-optical [16], or natural-optical [17]–[23] feedback loops to demonstrate self-oscillation. In such systems, DC electricity or unmodulated light is converted into harmonic power, making them particularly useful for MEMS clocks [24] or filters [25], if frequency instability is sufficiently low.

For MEMS resonators,[1] illuminated within an optical interference field, coupling between displacement and either photothermal stress [17]–[20], [22], [23], [26]–[29], electric charge [21], or light pressure [30]–[36] may lead to a natural closed feedback loop. The sign of the feedback gain is determined by the length of the interference cavity or wavelength of the light used for illumination. For negative feedback gain, damping of thermal vibrations occurs that decreases the quality factor and is termed cavity- or self-cooling [28], [32], [33]. For positive feedback gain, the back-action reduces damping resulting in a higher quality factor [37]. In this case, when the illumination power is increased beyond a threshold value, P_{Hopf}, the damping becomes negative, destabilizing the equilibrium configuration and leading to large amplitude self-sustained vibrations termed limit cycle oscillations (LCOs). Such devices have drawn attention due to applications in resonant sensing [15] and detection of gravity waves [38].

Since LCOs exhibit periodic motion in the absence of any external periodic forcing, their forced response is quite different than that of a resonator. When a LCO, operating with frequency f_{LCO}, is externally driven at a separate drive frequency, f_D, and drive amplitude, A_D, the type of response depends on the strength of forcing and the level of frequency detuning [39]–[41]. For hard forcing near the limit cycle frequency, the limit cycle will be entrained to respond at f_D whereas for soft forcing away from the limit cycle frequency, both f_D, and f_{LCO} will be seen in the frequency of the response. Thus, the frequency of response depends on the amplitude of the forcing. Super- and subharmonic entrainment may also occur when the f_D:f_{LCO} ratio is near 1:n and n:1, respectively. In this case, for sufficiently hard forcing near a super- or subharmonic resonance, the response frequency will be shifted to the nearest integer fraction or multiple of the drive frequency, respectively [39]–[42]. Hyugens originally

Manuscript received August 1, 2012; revised January 5, 2013; accepted January 27, 2013. Date of publication March 12, 2013; date of current version July 29, 2013. This work was supported by the National Science Foundation (NSF) under Grant 0600174, in part by the Cornell NanoScale Facility, a member of the National Nanotechnology Infrastructure Network, with support from the NSF, under Grant ECS-0335765, and in part by the Integrated Advanced Microscopy and Materials Facilities, Cornell Center for Materials Research with support from the NSF Materials Research Science and Engineering Centers program under Grant DMR 1120296. Subject Editor F. Ayazi.

D. B. Blocher is with the Department of Mechanical and Aerospace Engineering, Cornell University, Ithaca, NY 14853 USA (e-mail: dbb74@cornell.edu).

A. T. Zehnder is with the Cornell College of Engineering, Cornell University, Ithaca, NY 14853 USA (e-mail: atz2@cornell.edu).

R. H. Rand is with the Department of Mechanical and Aerospace Engineering and the Department of Mathematics, Cornell University, Ithaca, NY 14853 USA (e-mail: rhr2@cornell.edu).

Color versions of one or more of the figures in this paper are available online at http://ieeexplore.ieee.org.

Digital Object Identifier 10.1109/JMEMS.2013.2248124

[1]We use the term oscillator to refer to a device that exhibits sustained periodic motion, and resonator to refer to a device characterized by damped periodic motion. In addition, we use the term natural feedback to refer to feedback due to intrinsic device physics, and active feedback to refer to feedback due to external electronics.

discovered primary-entrainment[2] in the 1600s while studying pendula clocks. Mathematical analyses of LCOs themselves were later developed by Van der Pol [43], who also discovered higher order entrainment while studying relaxation oscillations in electrical circuits [42].

Models of primary entrainment typically result in sharply defined V-shaped regions of entrainment in the $f_D - A_D$ parameter space emanating from $(f_{\mathrm{LCO}}, 0)$ [39]–[41]. In this picture, for a (f_D, A_D) inside the V, the limit cycle is entrained, if outside the V the limit cycle is not entrained. In addition, no matter how small the drive amplitude, A_D, a drive frequency f_D sufficiently close to f_{LCO} will guarantee entrainment. Prior modeling and experimental work on LCOs in MEMS has illustrated hysteresis in the region of entrainment [44]–[47], a tilt toward higher frequency of primary entrainment at higher drive amplitudes in amplitude-hardening limit cycles [45], and explored the regions of subharmonic entrainment in a force relaxation oscillator [48].

Natural limit cycles were first demonstrated in a MEMS device by Langdon and Dowe [17]. Zalalutdinov *et al.* [44]. later demonstrated the use of 1:1 and 2:1 entrainment to reduce the frequency instability of a LCO to that of a highly stable external drive. Inertial drive was used to obtain 1:1 entrainment and 2:1 entrainment was obtained by amplitude modulation of the laser power. Feng *et al.* [9]. demonstrated 1:2 entrainment in mechanically-coupled cantilevers driven piezoelectrically.

Extensive work exists on the related phenomena of subharmonic and superharmonic resonance, where a resonator (i.e., not self-oscillating) shows a large amplitude response when driven at a frequency near a multiple or submultiple of its natural frequency. Unlike the case of entrainment of an LCO, the response frequency does not depend on the drive amplitude for such resonances. Shim *et al*. demonstrated superharmonic resonance up to 1:7 in addition to other resonances in mechanically-coupled MEMS beams [10].

Finally, if periodic forcing modulates a system parameter (such as the stiffness), parametric resonance may occur where the resonator response amplitude is a discontinuous function of the drive frequency [41], [49]. This effect is most prominent for forcing near twice the natural frequency, and the resulting separation in drive and detection frequencies has been used to prevent capacitive coupling in RF electronics [50].

While this and past experimental work [44] uses an external stable frequency source to reduce the frequency instability of the LCO, recent theoretical work has focused on increasing frequency precision [51] or reducing frequency instability via coupling of multiple oscillators [52]. As such, experimental work on entrainment of a noisy LCO via a stable external drive is one step toward on-chip coupling of multiple noisy LCOs. Though our work makes use of natural optical feedback to obtain self-oscillation, it is equally applicable to oscillators using active optical [53] or electronic feedback [15].

We show experimentally that for a noisy LCO, entrainment is an inherently statistical phenomenon, and hard forcing is required to get persistent locking. This result is in contrast to the traditional analysis of sharply defined V-shaped regions of entrainment. In addition, experimental data show that for doubly and singly supported beams of the same length, the size of the region of primary entrainment and the order of sub- and superharmonic entrainment attainable are dramatically different. Modeling suggests that this difference may be caused by the differing level of displacement nonlinearity in singly and doubly supported beams.

In the following sections, the fabrication and characterization of devices tested is described, as are the experimental setup and procedures. Then, experimental results are presented and discussed, followed by a review of prior modeling work and an extension of that work to the current experimental data. This paper focuses on the juxtaposition of devices with and without amplitude–frequency relationships and the affect of frequency instability on entrainment.

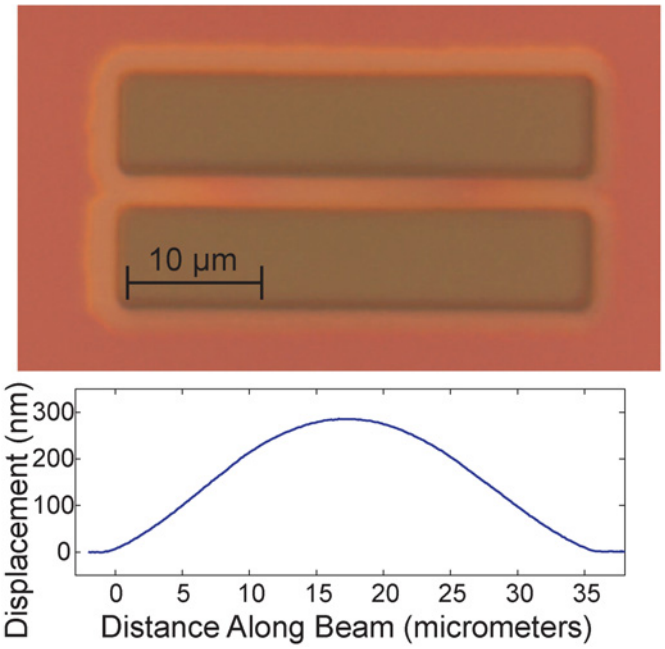

Fig. 1. Microscope image of a 35 μm doubly supported device. Overlayed is a plot of the out-plane displacement measured using optical profilometry. The bare substrate appears brown, while the beam and undercut support appear orange. Singly supported devices (not pictured) are free on one end.

II. Setup and Procedure

Devices are fabricated out of single crystal silicon using a silicon-on-insulator (SOI) process. Singly and doubly supported beams, 2μm wide and 7–40 μm long, are patterned using photolithography and defined with dry etching. Beams are aligned along the crystal symmetry planes of Si in order to avoid bending–twisting coupling [54]. Devices are released with a wet etch and critical point drying is used to avoid stiction. Final device thickness is measured to be 201 nm. SEM imaging and optical profilometry indicate that doubly supported beams, 15 μm and longer, are buckled up due to residual compressive stress in the device layer. In doubly supported beams, midplane stretching [55] leads to amplitude-hardening in prebuckled beams [56] due to a nonlinear load–

[2]The term primary is used to denote 1:1 entrainment as distinct from higher order sub- or superharmonic entrainment.

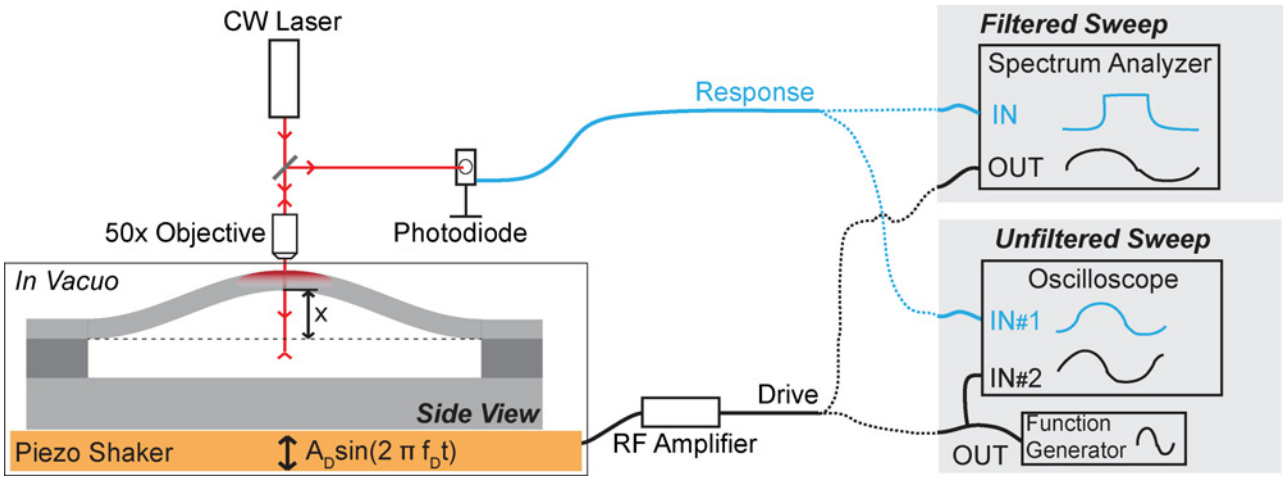

Fig. 2. Diagram of experimental setup. The gap between the beam and substrate below forms a Fabry–Pérot interferometer. Deflection of the beam x changes the fraction of light absorbed, leading to self-oscillation in the first bending mode when the laser power is higher than a threshold value, P_{crit}. Modulation of the reflected light is measured in a high-speed photodiode and used to transduce motion. Beams may also be driven inertially through the piezoshaker.

displacement curve, and amplitude-softening in postbuckled beams [57] due to symmetry breaking. The following discussion and the data presented here are for 35 μm long singly and doubly supported beams. This length of beams was selected for the low P_{Hopf} value in doubly supported beams, allowing us to study illumination at $P >> P_{\text{Hopf}}$.

Devices are indium bonded to a piezoelectric disk, used to provide inertial drive, and loaded into a high vacuum chamber evacuated to 10^{-7} mbar to effectively eliminate viscous damping. A continuous wave HeNe laser is focused to a $\sim 5\,\mu$m diameter spot on the devices using a microscope, and interferometric drive and detection is used to induce LCOs and transduce their motion (see Fig. 2). Further details can be found in [58]. Singly supported beams are illuminated near their tip and doubly supported beams at their midline.

The beams are observed to spontaneously transition into LCO at their first mode frequency when the laser power on sample is increased beyond $P_{\text{crit}} = 75\ \mu$W for doubly supported beams and $P_{\text{crit}} = 480\ \mu$W for singly supported beams, respectively. Further increase in the laser power increases the amplitude of oscillation. The doubly supported beams are seen to be amplitude-softening: with the frequency of oscillation decreasing from 1.93 MHz at the minimum detectable laser power down to 1.68 MHz at 1785 μW on sample. In addition, a high level of frequency instability is observed in doubly supported beams with a sweep-to-sweep deviation in frequency of $\frac{\Delta f}{f} = 4 \times 10^{-3}$ measured at 1050 μW with $\tau = 161$ ms sweep time. Singly supported beams are seen to be highly linear and stable, with frequency detuning of only -0.023% as the amplitude varies over three orders of magnitude, and a frequency deviation of $\frac{\Delta f}{f} = 3 \times 10^{-5}$ measured at 700 μW. See the insets of Figs. 6 and 9 for the measured amplitude–frequency relationships in doubly and singly supported beams, respectively—the curve describing this relationship is termed the backbone curve [41].

To study entrainment, the laser power on sample is increased beyond P_{crit} to a fixed power so that the devices exhibit LCO at fixed Frequency, f_{LCO}. Then, the self-oscillating devices

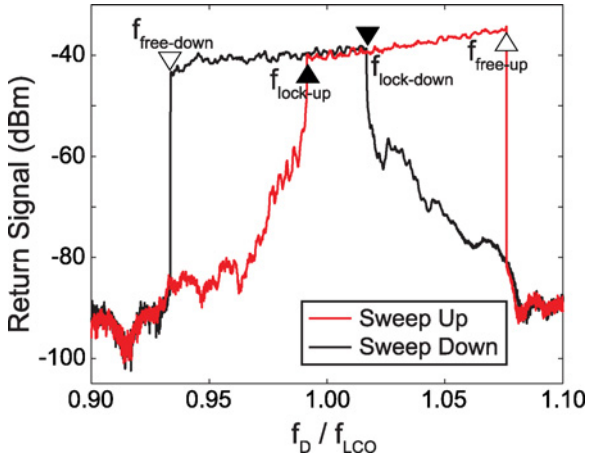

Fig. 3. Sample data showing measured region of 1:1 entrainment using filtered-sweeps. Upward sweep is in red, and downward sweep in black. Note the logarithmic y-scale. Amplitude of motion is not proportional to the return signal due to nonlinearities in the detection scheme. Thus, the amplitude of motion cannot be inferred from spectral data alone. See [59] for a description of the methodology used to obtain calibrated displacement data.

are driven inertially with the piezoelectric disk at a separate drive frequency, f_D. Thus, the unmodulated laser creates a limit cycle and the periodic inertial drive is used to entrain it. Entrainment is measured in terms of either frequency-matching or phase locking. The first method employed, termed filtered-sweep, uses the spectrum analyzer as both the source for the drive signal and the instrument for measuring the frequency content of the motion. The spectrum analyzer outputs a swept sine wave that is fed through a high-frequency amplifier and applied to the piezoelectric drive disk. The peak-to-peak voltage across the piezo is recorded and is used as a measure of the drive amplitude, A_D. The response signal from the photodiode is input into the spectrum analyzer and filtered at the drive frequency (see Fig. 2). When the limit cycle is entrained, the response and drive frequencies match, the response signal passes through the filter, and a large amplitude response is measured. When entrainment is lost, the response

frequency does not match the drive frequency and is filtered out, leading to a low amplitude signal. Thus, the measured response is a plateau whose endpoints show the frequency at which entrainment begins and ends (see Fig. 3): note that the region of entrainment depends on the direction of sweep [44], [45]. The sweep rate is kept low enough ($\leq$ 0.2%/s) that the frequency may be assumed to change quasistatically, and the finite width bandpass filter limits measurements to regions of entrainment wider than 2 kHz. This method is precise and automatable, allowing for measurement of the statistics of entrainment for weak forcing. Measured deviation in the drive signal frequency is less than $\frac{\Delta f}{f} = 5 \times 10^{-7}$, but total harmonic distortion up to 10% (power ratio) is seen at the highest drive amplitude due to limitations of the RF amplifier.

For sub- and superharmonic entrainment, the response is at an integer multiple or fraction of the drive frequency, and an unfiltered-sweep is used to measure entrainment in terms of phase locking (see Fig. 4). A function generator supplies the swept sine drive signal and a frequency counter is used to accurately track its frequency. Drive and response signal are viewed on an oscilloscope: when entrained, the signals are phase locked and the response will appear coherent when triggering on the drive; when entrainment is lost, the response phase will drift with respect to the drive and appear as high amplitude noise. Using this method, frequency instability of the swept sine from the function generator limits measurements to regions of entrainment wider than $\sim$ 0.5 kHz. Note that this width is an order of magnitude smaller than the measured frequency instability of the limit cycle itself.

III. Results

At low drive amplitude, self-oscillating doubly supported beams were seen to jump in and out of entrainment for a fixed drive frequency and amplitude. To study the statistics of entrainment, we measured the region of entrainment for 100 successive sweeps using a filtered sweep with sweep rate of 1kHz/s. The laser power is set to P = 1050 μW on sample, giving mean frequency f_{LCO} = 1.63 MHz. The points at which locking starts and stops vary from sweep to sweep, and on a given sweep the oscillator moves in and out of entrainment (i.e., multiple plateaus). Statistics of entrainment are given in Fig. 5. For the lowest drive amplitude plotted, A_D = 0.078 V, there is no drive frequency for which the oscillator is entrained on every sweep. Note that the range of frequencies, for which statistics are important, is orders of magnitude larger than the measured frequency deviation of $\frac{\Delta f}{f} = 4 \times 10^{-3}$. As the drive amplitude is increased, the width of the region of entrainment grows and the boundaries become sharp. For A_D = 0.622 V, the statistical nature of entrainment has become insignificant.

For a larger range of forcing amplitudes, the region of 1:1 entrainment was measured with laser power on sample of 105, 525, and 1050 μW. See Fig. 6 for results—points plotted are the average of two unfiltered sweeps. It has been shown that an amplitude-hardening limit cycle oscillator is constrained to the backbone curve when entrained, giving asymmetry in the region of entrainment with a right tilted V shape [44], [45]. Here, we see that the same is true for amplitude-softening limit

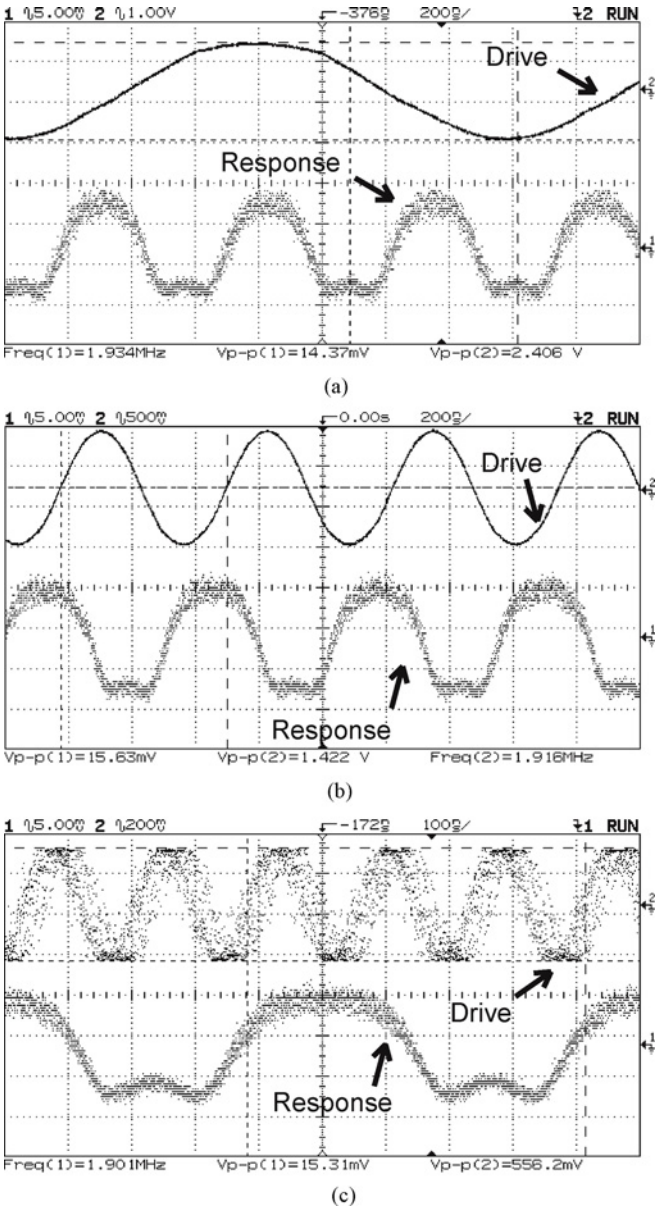

Fig. 4. Oscilloscope traces showing 1:3, 1:1, and 3:1 entrainment. Signal from the photodiode (response) is plotted along with the input to the piezoshaker (drive). Note that for 1:n entrainment, the response completes exactly n cycles in the time the drive goes through one cycle. The flattening of the trough in the response is due to the motion of the beam through a peak in the optical interference field, moving power in the reflected signal into 2f and higher harmonics. For n:1 subharmonic entrainment, at given phase in the drive the limit cycle is at one of n different phases, thus we trigger on the return signal. As a result, the drive signal appears noisy due to noise in the (triggered) response signal. (a) 1:3 Superharmonic entrainment. (b) 1:1 Primary entrainment. (c) 3:1 Subharmonic entrainment.

cycle oscillators with the direction of tilt switched. In addition, by selecting our operating point, we can tune the level of asymmetry in the region of entrainment. Examining the data for P = 105 μW, we see that when sweeping up in frequency, locking does not occur until f_D is very close to f_{LCO}, and then is quickly lost. When sweeping down, locking persists as the limit cycle is detuned by -15%. Changing the laser power changes the location of the oscillator on the backbone curve, with higher laser powers yielding lower frequencies and

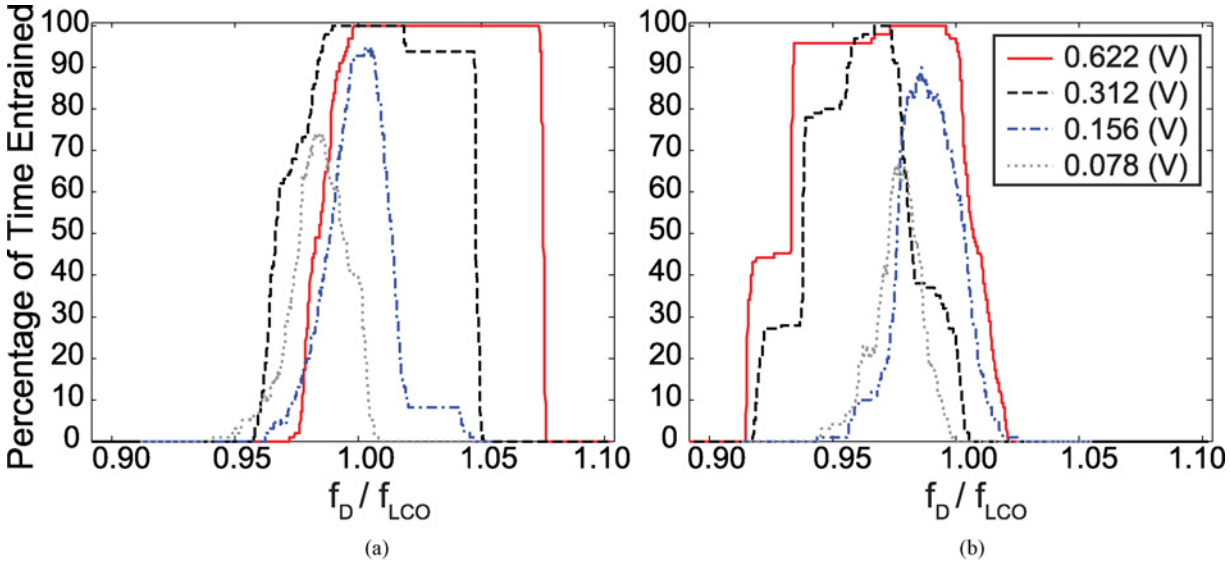

Fig. 5. Measured statistics of 1:1 entrainment for a 35 μm doubly supported beam with P = 1050 μW on sample. The drive amplitude (A_D) was held fixed, as the drive frequency (f_D) was repeatedly swept between 90% and 110% of the limit cycle frequency. Plotted is the percentage of sweeps during which the limit cycle was entrained at a given frequency of drive. Drive frequency is normalized by the undriven limit cycle frequency, f_{LCO}, and lines show data for various drive amplitudes. (a) Sweep up. (b) Sweep down.

a locally flat amplitude–frequency relationship. Higher up the backbone curve, the region of entrainment still shows hysteresis but is less asymmetric. This effect has been previously noted in a research letter [44], though data were not presented.

Initial results showed that the order of sub- or superharmonic entrainment attainable for the device did not depend on the laser power used and so these regions were measured at the single laser power of P = 1050 μW. See Figs. 7 and 8 for results. Superharmonic entrainment of order 1:7 is only observed in the doubly supported beam at the highest achievable drive level, and 1:8 entrainment is not seen. Care must be taken to ensure that we truly measure 1:n superharmonic entrainment via the drive signal at f_D and not primary entrainment via the small harmonic distortion at $n \times f_D$. Our measured regions of superharmonic entrainment are significantly wider than the measured region of 1:1 entrainment with drive amplitude scaled by harmonic distortion, ruling out the latter scenario. Subharmonic entrainment of order 3:1 was seen for a range of forcing levels, while 4:1 or higher was not seen. The largest region of entrainment at a given forcing level was seen for 1:1 forcing, where energy transfer is most efficient. Finally, we note that superharmonic entrainment is seen to occur at a frequency slightly less than $(1/n)f_{\mathrm{LCO}}$. Amplitude-hardening devices have previously been shown to entrain at higher frequencies as the drive amplitude increases [45]. Thus, we believe that the measured frequency shift to lower frequencies for superharmonic entrainment in our device is related to the amplitude-softening of the device combined with a frequency-dependent piezoshaker having greater output at lower frequencies. However, more work is needed to determine the exact cause.

Primary entrainment was also observed in 35 μm singly supported beams over a narrow range of frequencies, and is shown in Fig. 9 along with a plot of the amplitude–frequency relationship. Due to their relative compliance and low resonant frequency, the drive amplitude for singly supported beams was limited by the 400-nm gap between device and substrate rather than harmonic distortion. However, data are plotted for the same range of forcing levels as the doubly supported beams. Note that the width of the entrainment region at a given forcing level is orders of magnitude lower in the singly supported beams (see Fig. 9) than the doubly supported beams (see Fig. 6). Direct comparison of drive amplitudes between singly and doubly supported beams is tenuous due to the difference in resonant frequencies, combined with the frequency-dependent mechanical and electrical impedance of the piezodisk and drive electronics, respectively. However, sub- and superharmonic entrainment were not seen for any forcing amplitude in singly supported devices.

IV. Modeling

Prior analytic work on entrainment of optically transduced MEMS limit cycle oscillators has been performed by Zalalutdinov *et al.* [44] and Pandey *et al.* [45], who examined entrainment via inertial drive and laser power modulation. Experimental results for a disk-shaped oscillator [44] were fit using a 10-parameter model derived in [18]. First mode vibration was assumed, and a lumped parameter thermal model governing the average temperature, T, was coupled to a nonlinear oscillator model governing the displacement at the point of illumination, z. The model exhibited amplitude-hardening and parametric forcing via external modulation of the laser power in addition to direct inertial forcing.

Integration of the model equations for 1:1 inertial forcing matched experimental data [45], with a right tilted V-shaped region, significant asymmetric hysteresis, and a corner in the graph of $f_{\text{free-up}}$. These qualities were attributed to amplitude-hardening of the limit cycle. Further simulations indicated that a parametric term was required to obtain 2:1 entrainment via

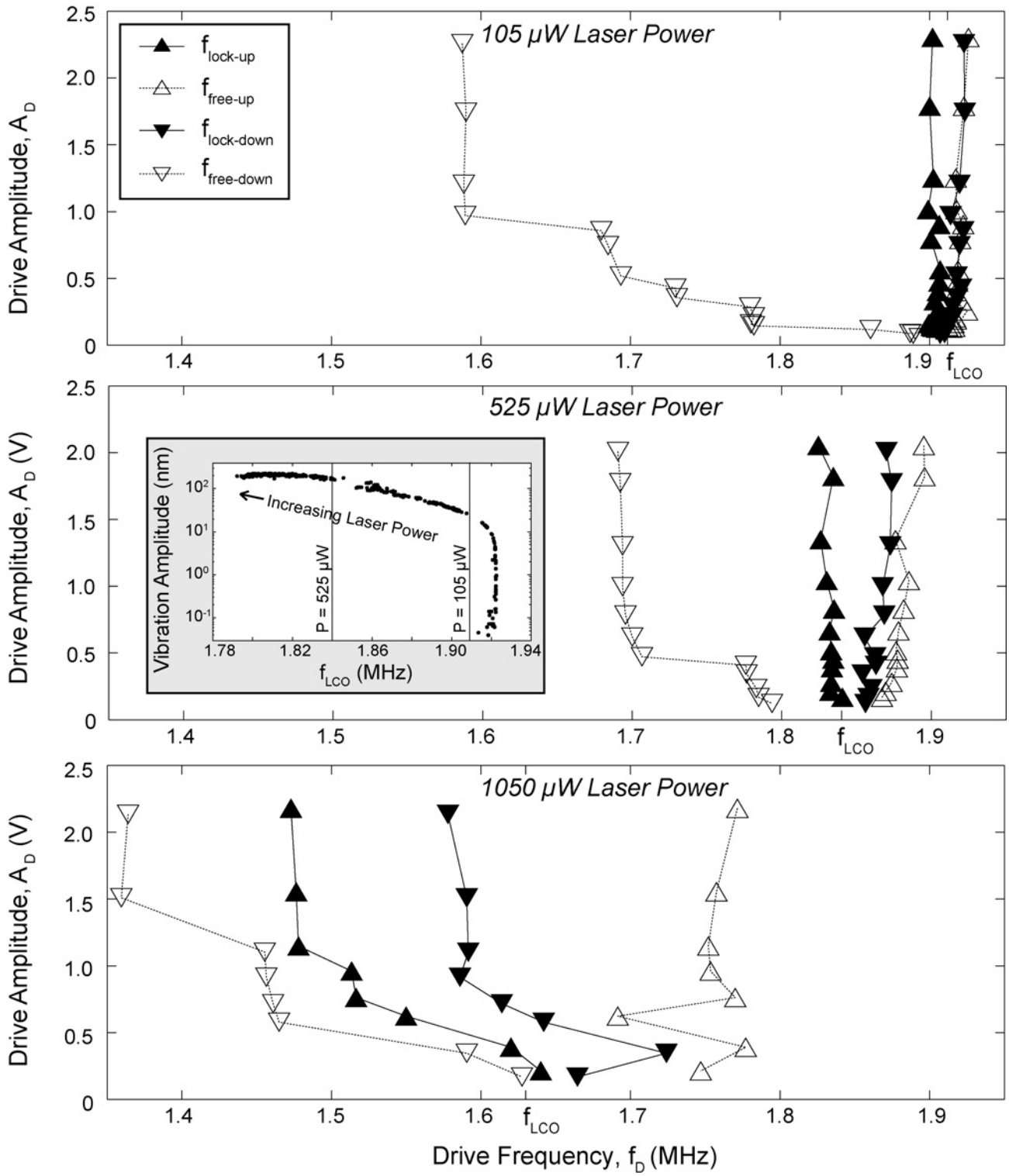

Fig. 6. Measured region of 1:1 entrainment in a 35 μm doubly supported beam as a function of laser power on sample. A_D is held fixed, while f_D is swept up and down quasi-statically. Plotted are the points at which entrainment begins (closed triangle) and ends (open triangle), for a given drive amplitude and direction of sweep. Note that the region of entrainment depends on the direction of sweep. (Inset) Data showing the amplitude–frequency relationship, i.e., backbone curve, measured by continuously increasing the laser power beyond the Hopf, with no external forcing. For $P = 1050$ μW, the frequency of oscillation is 1.63 MHz (not shown).

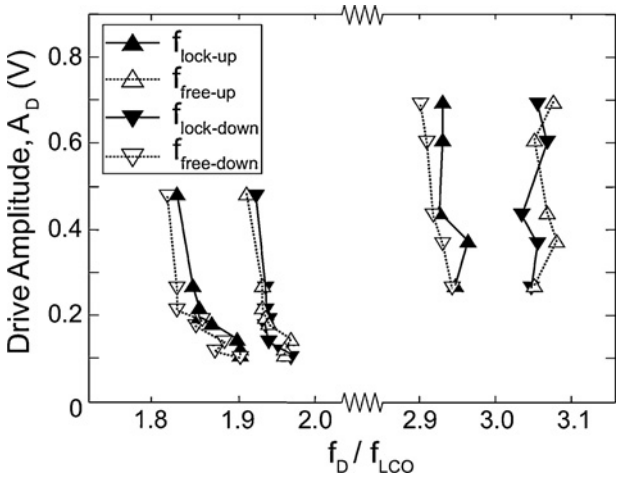

Fig. 7. Measured regions of subharmonic entrainment in a 35 μm doubly supported beam. The drive frequency f_D is normalized by the undriven limit cycle frequency f_{LCO}.

laser modulation, and that increasing the CW laser power shifted the region of 1:1 entrainment under inertial forcing, but did not change the level of hysteresis or asymmetry of the region. A perturbation analysis of the same model equations was performed in [46].

In [47], a simpler forced Mathieu-van der Pol-Duffing model was considered, which reproduces the essential features of experimental data in [44]: LCOs (van der Pol term), an amplitude–frequency relationship (Duffing term), and parametric forcing (Mathieu term). Perturbation theory was used to derive the slow flow equations assuming no parametric forcing, and numerical continuation of the slow flow for an amplitude-hardening limit cycle indicated partial hysteresis, specifically a distinction between $f_{\text{free-up}}$ and $f_{\text{lock-down}}$ but not between $f_{\text{free-down}}$ and $f_{\text{free-up}}$.

In this paper, we attempt to explain the measured difference in entrainment regions between singly and doubly supported beams, specifically that doubly supported beams display significant hysteresis and asymmetry in a wide region of 1:1 entrainment and support sub- and superharmonic entrainment. Model equations are not intended to accurately reproduce all experimental data, but rather to explain a specific aspect of it. The qualitative features of the experiments that our model reproduces are an LCO (van der Pol term), and a stiffness nonlinearity (Duffing term). We assume first mode vibration, and model our system as a forced van der Pol-Duffing oscillator. Letting the centerline displacement (or tip deflection) be x, we get the following differential equation:

$$\ddot{x} + x - c\left(1 - x^2\right)\dot{x} + \beta x^3 = A_D \cos\left(2\pi f_D t\right) \qquad (1)$$

where A_D and f_D are the drive amplitude and frequency. The van der Pol term, $c\left(1-x^2\right)$ produces a limit cycle of amplitude 2 [41], with c determining its shape and strength. The Duffing term, βx^3, leads to an amplitude–frequency relationship in the undamped system ($c = 0$), with the magnitude of the nonlinear stiffness, β, determining the strength of the relationship. The Duffing term also leads to an anharmonic response for large amplitude or large nonlinearity. Units in (1) are as follows: 1) time is nondimensionalized such that the device has linear resonant frequency of 1; and 2) displacement is nondimensionalized by the measured limit cycle amplitude (discussed later). Model equations are a simplification of those presented in [47]. For doubly supported beams that support tension across their length, the linear stiffness is temperature dependent, thus, forcing via laser modulation will parametrically drive the device. When forcing is inertial (as in our case), out-of-plane displacement will modulate the absorptive heating, and thus the stiffness, however, this is a second-order effect. Thus, we drop the parametric term from [47].

In order to determine c, we set β and $A_D = 0$ and integrate (1) to steady state. For $c \gg 1$, a strong limit cycle exists with anharmonic shape and two-time scale motion (i.e., relaxation oscillation). For $c \ll 1$, the limit cycle is weak but sinusoidal. Low-amplitude LCOs in our devices are seen to be nearly sinusoidal with frequency-tuning and shape of the motion coming from the nonlinear stiffness. Thus, we select c = 1/100, whereby the limit cycle is sinusoidal to within 0.2% for $\beta = 0$.

To determine the nonlinear stiffness, β, we set $c = 0$ and least squares fit the analytic approximation for the backbone curve of a Duffing oscillator [41] to the measured data (inset Fig. 6). We select units of x to be $(x) = 50\,\text{nm}$ so that the model limit cycle amplitude of 2 corresponds to an amplitude of 100 nm in the physical device, giving $\beta_{eff} = -0.032\frac{1}{(x)^2}$ for doubly supported beams. The nonlinear stiffness for singly supported beams is effectively zero (see the measured amplitude–frequency relationship in Fig. 9).

To examine the effects of stiffness nonlinearity on the regions of primary, sub-, and superharmonic entrainment, (1) is integrated for a range nonlinearities, $\beta = \beta_{\text{eff}}$, $0.5 \times \beta_{\text{eff}}$ and $0.1 \times \beta_{\text{eff}}$, between that of our doubly supported beams (β_{eff}) and singly supported beams ($\beta = 0$). Results for $\beta = 0.1 \times \beta_{\text{eff}}$ were only slightly different from those for $\beta = 0$ and thus the former was chosen as a lower bound. For a given drive amplitude, A_D, we step the angular drive frequency, $2\pi f_D$, in increments of $1 \times 10^{-4} - 1 \times 10^{-3}$, integrate to steady state, and seed the initial condition of the next frequency step using the solution for the current step. The steady state solution is sampled 2^{13}–2^{18} times over 2^8–2^{12} periods, and the Fourier transform taken: when entrained, the spectral content of the response shows peaks at f_D and its harmonics; when not entrained, sidebands are seen in the response in addition to peaks at f_D and f_{LCO}.

Integration results for 1:1 entrainment are plotted in Fig. 10. For $A_D = 0.2$ the width of the region of entrainment with $\beta = \beta_{\text{eff}}$ is approximately equal to the maximum width measured experimentally in our doubly supported devices; thus, we restrict forcing levels in the model to $A_D \leq 0.2$. For $A_D \geq 0.25$ with $\beta = \beta_{\text{eff}}$, the limit cycle is seen to be rendered unstable at certain detunings and trajectories escape to infinity—an unphysical feature of the model. Note that reducing β shrinks the region of primary entrainment for a given forcing level. For sufficiently small β, the nonlinear stiffness has negligible effect on the region of 1:1 entrainment, which reduces to that of the van der Pol model alone. While hysteresis is present in the model for high β, we note that:

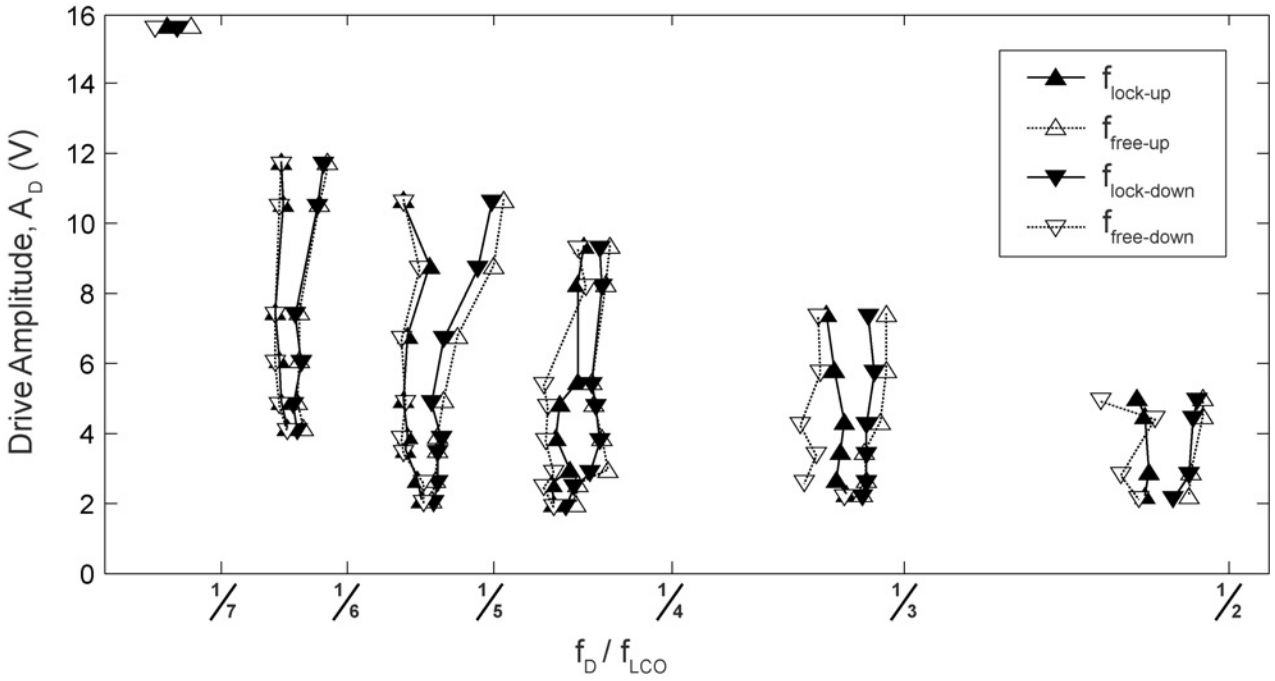

Fig. 8. Measured regions of superharmonic entrainment in a 35 μm doubly supported beam. The drive frequency f_D is normalized by the undriven limit cycle frequency f_{LCO}. A logarithmic frequency scaling is used in order to display all measured regions on a single plot. Note that 1:n superharmonic entrainment occurs at a frequency less than $(1/n)f_{LCO}$.

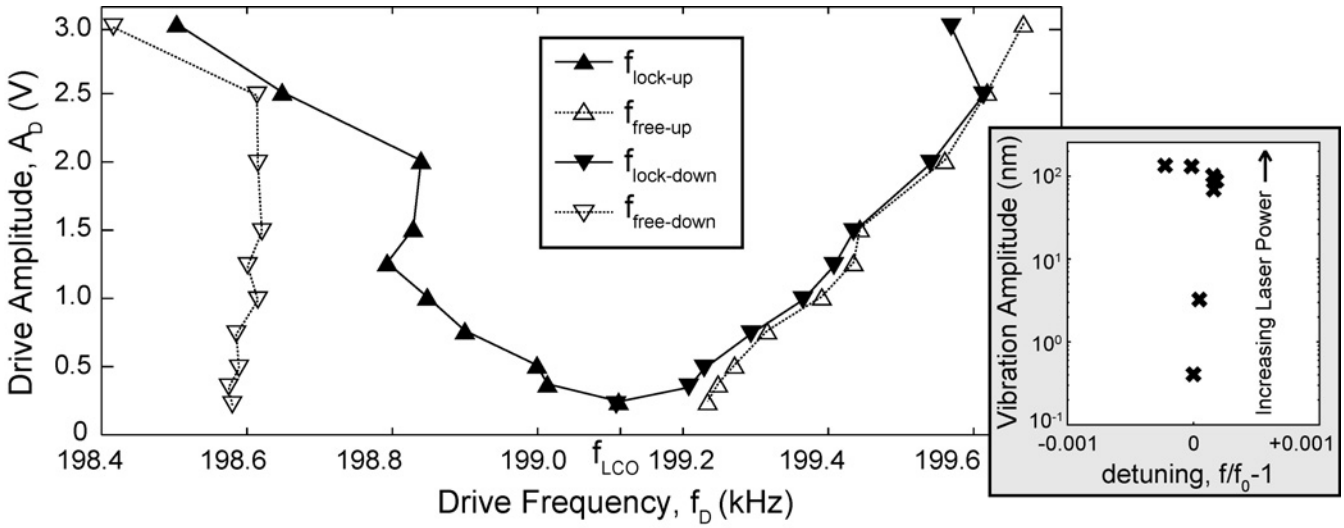

Fig. 9. Measured region of 1:1 entrainment in a 35 μm singly supported beam. (Inset) Data showing the measured amplitude–frequency relationship.

it is not present to the same extent seen in experimental results; the model does not appear to distinguish between $f_{\text{lock}-\text{up}}$ and $f_{\text{free-down}}$ until the forcing reaches a critical level; and numerical integration shows a slight distinction between $f_{\text{lock-down}}$ and $f_{\text{free-up}}$ for hard forcing with strong nonlinear stiffness.

We also examine the region of sub- and superharmonic entrainment in the model for the maximum forcing level of $A_D = 0.2$. Frequency steps were scaled by order of entrainment such that the minimum step measured at the response frequency was $5\times10^{-5}\times f_{\text{LCO}}$. Using the two variable expansion perturbation method, the cubic Duffing nonlinearity only produces resonant terms for 1:3 and 3:1 entrainment. Sub- or superharmonic entrainment at other orders were not detected in this simple model using direct numerical integration with the minimum frequency step and maximum forcing level. See Table I for results—note that the width of the sub- and superharmonic entrainment regions are a strong function of the level of stiffness nonlinearity. Significant hysteresis was not seen.

While use of a cubic stiffness term, βx^3, to produce an amplitude–frequency relationship is traditional, it has limitations.[3] A cubic term can be amplitude-softening or hardening

[3]The use of the van der Pol term to create a limit cycle in the dynamics is also common, though this formulation is not unique. Further work might explore the impact this choice has on model predictions.

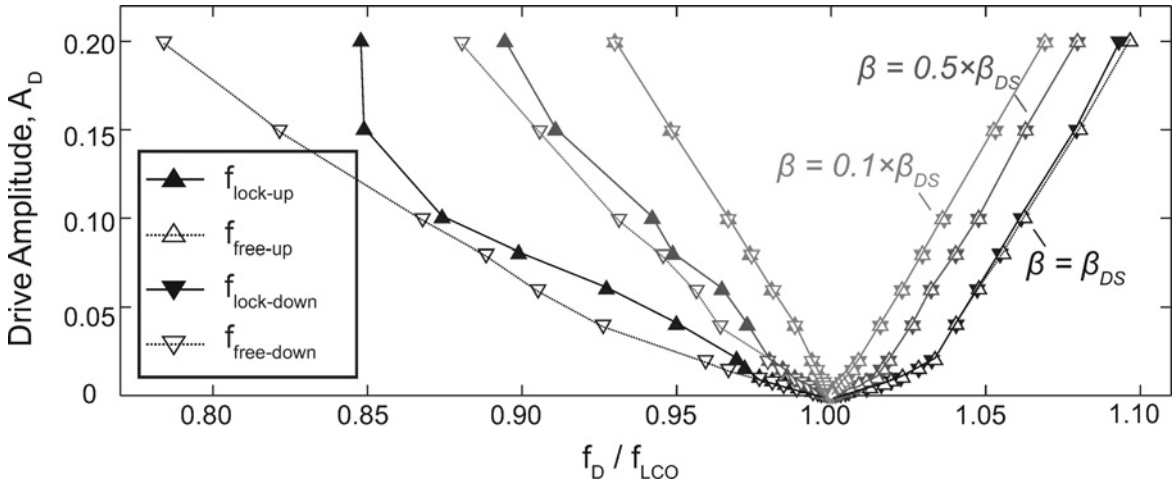

Fig. 10. Predicted region of 1:1 entrainment for 1 as the nonlinear stiffness β is decreased. Results are calculated using direct numerical integration. Results for $\beta = 0$ (not shown) were found to be similar to those for $\beta = 0.1 \times \beta_{\text{eff}}$.

TABLE I

REGIONS OF 1:3, 1:1, AND 3:1 ENTRAINMENT IN CUBICALLY NONLINEAR MODEL (1) AS A FUNCTION OF NONLINEAR STIFFNESS, β, FOR FIXED FORCING LEVEL, $A_D = 0.2$. DRIVE FREQUENCIES ARE NORMALIZED BY f_{LCO}

	β_{eff}	$0.5\times\beta_{\text{eff}}$	$0.1\times\beta_{\text{eff}}$
1:3 Region	[2.9750–3.0139]	[2.9946–3.0054]	[2.9997–3.0007]
1:1 Region	[0.84781–1.0930]	[0.89441–1.0797]	[0.92996–1.0691]
3:1 Region	[0.33278–0.33308]	N/A	N/A

TABLE II

REGIONS OF SUB- AND SUPERHARMONIC ENTRAINMENT IN MODEL WITH QUADRATIC AND CUBIC NONLINEARITIES (2) FOR FIXED FORCING LEVEL, $A_D = 0.2$ (DRIVE FREQUENCIES ARE NORMALIZED BY f_{LCO})

Order of Entrainment	1:3	1:2	2:1	3:1
Region	[2.9967–3.0039]	[1.9360–2.0610]	[0.489750–0.508500]	[0.332800–0.333767]

depending on the sign of β and preserves the (odd) symmetry. However, for a beam in the buckled state, the symmetry is broken due to the presence of the (unstable) unbuckled state and other (stable) buckled state to one side of the configuration. This produces a quadratic stiffness [57], αx^2, which is always softening in addition to the cubic stiffness [60], [61], and produces even harmonics in the motion for large amplitude. Competition/collaboration between quadratic softening and cubic hardening/softening yields an equivalent (cubic) nonlinearity $\beta - \left(\frac{10}{9\omega_o^2}\right)\alpha^2$. Assuming that half of the amplitude-softening comes from the quadratic nonlinearity and half from the cubic, we get

$$\ddot{x} + x - c\left(1 - x^2\right)\dot{x} + \sqrt{\frac{-9\beta_{eff}}{20}}x^2 + \frac{\beta_{eff}}{2}x^3 = A_D \cos\left(2\pi f_D t\right). \quad (2)$$

To lowest order, (2) has the same backbone curve as (1) with $\beta = \beta_{eff}$ [40], [41], [62]. Our analysis of sub- and superharmonic entrainment was repeated using (2), and results are presented in Table II. Inclusion of the quadratic nonlinearity produces resonant terms that allow for 1:2 and 2:1 entrainment in the model, though other orders of entrainment are still not seen for the minimum frequency step used.

V. CONCLUSION

In this paper, we contrasted entrainment in optically self-resonant 35 micrometer doubly supported and singly supported beams. Doubly supported beams were seen to be buckled leading to a strong amplitude–frequency relationship. This allowed for considerable frequency tuning of the limit cycle with laser power, but also allowed for laser power instability to be mapped into frequency instability via the (power)–amplitude–frequency relationship. In contrast, singly supported beams showed orders of magnitude less frequency tuning and frequency instability. Results indicated a tradeoff between tunability and noise in self-resonant devices.

Self-oscillating devices were inertially driven and regions of primary, sub- and superharmonic entrainment measured. We demonstrated for the first time the effect of frequency instability on the region of 1:1 entrainment showing that in the presence of frequency instability, the limit cycle may jump in and out of entrainment for a fixed forcing frequency and amplitude, and that hard forcing is required to get persistent locking. In addition, the range of frequencies over which transient locking was measured was much larger than the variation in frequency of the limit cycle itself, illustrating how disruptive frequency instability was to entrainment. Results suggested that in order for entrainment to be a viable means

of reducing frequency instability, forcing (i.e., coupling) must be sufficiently strong to prevent transient locking.

A wide region of 1:1 entrainment was measured for doubly supported devices, with considerable hysteresis and asymmetry, as well as sub- and superharmonic entrainment at orders from 3:1 to 1:7. Singly supported beams exhibited a narrow region of 1:1 entrainment and no measurable sub- or superharmonic entrainment. Subsequent modeling suggested that frequency tunability in the doubly supported beam made possible by nonlinear stiffness allows for a wide region of 1:1 entrainment as well as high-order sub- and superharmonic entrainment. In the model, the effect of nonlinear stiffness on the width of and hysteresis in the region of 1:1 entrainment was modest, though the increase in the width of sub- and superharmonic entrainment with nonlinearity is pronounced. Our simple model does not reproduce entrainment of every order measured. In particular, an even ordered nonlinear stiffness term is needed to capture even ordered entrainment, suggesting that the traditional use of a cubic stiffness to produce an amplitude–frequency relationship is insufficient to capture high-order entrainment, and full expansion of the load curve is important. We noted, however, that no parametric term was included that was shown in the past to allow for 2:1 laser entrainment.

REFERENCES

[1] K. Thornton, D. Uttamchandani, and B. Culshaw, "Temperature dependence of resonant frequency in optically excited diaphrams," *Electron. Lett.*, vol. 22, no. 23, pp. 1232–1234, Nov. 1986.

[2] K. Thornton, D. Uttamchandani, and B. Culshaw, "Novel optically excited resonant pressure sensors," *Electron. Lett.*, vol. 24, no. 10, pp. 573–574, May 1988.

[3] G. Kovacs, *Micromachined Transducers Sourcebook*. New York NY, USA: McGraw-Hill, 1998.

[4] T. Thundat, P. Oden, and R. Warmack, "Microcantilever sensors," *Microscale Thermophys. Eng.*, vol. 1, no. 3, pp. 185–199, 1997.

[5] B. R. Ilic, D. A. Czaplewski, H. G. Craighead, P. Neuzil, C. Campagnolo, and C. A. Batt, "Mechanical resonant immunospecific biological detector," *Appl. Phys. Lett.*, vol. 77, no. 3, pp. 450–452, 2000.

[6] Y. Yang, C. Callegari, X. Feng, K. Ekinci, and M. Roukes, "Zeptogram-scale nanomechanical mass sensing," *Nano Lett.*, vol. 6, no. 4, pp. 583–586, 2006.

[7] P. Waggoner and H. Craighead, "Micro- and nanomechanical sensors for environmental, chemical, and biological detection," *Lab Chip*, vol. 7, no. 10, pp. 1238–1255, 2007.

[8] S. Adams, F. Bertsch, K. Shaw, P. Hartwell, F. Moon, and N. MacDonald, "Capacitance based tunable resonators," *J. Micromech. Microeng.*, vol. 8, no. 1, pp. 15–23, 1998.

[9] J. Feng, X. Ye, M. Esashi, and T. Ono, "Mechanically coupled synchronized resonators for resonant sensing applications," *J. Micromech. Microeng.*, vol. 20, no. 11, pp. 115001-1–115001-5, 2010.

[10] S.-B. Shim, M. Imboden, and P. Mohanty, "Synchronized oscillation in coupled nanomechanical oscillators," *Science*, vol. 316, no. 95, pp. 95–99, 2007.

[11] T. S. Lammerink, M. Elwenspoek, and J. H. Fluitman, "Optical excitation of micro-mechanical resonators," in *Proc. IEEE Micro Electro Mech. Syst.*, Jan.–Feb., 1991, pp. 160–165.

[12] B. R. Ilic, S. Krylov, M. Kondratovich, and H. G. Craighead, "Optically actuated nanoelectromechanical oscillators," *IEEE J. Sel. Topics Quantum Electron.*, vol. 13, no. 2, pp. 392–399, Mar.–Apr. 2007.

[13] B. R. Ilic, S. Krylov, and H. G. Craighead, "Theoretical and experimental investigation of optically driven nanoelectromechanical oscillators," *J. Appl. Phys.*, vol. 107, no. 3, pp. 034311-1–034311-13, 2010.

[14] R. M. Fatah, "Mechanisms of optical activation of micromechanical resonators," *Sens. Actuators A, Phys.*, vol. 33, no. 3, pp. 229–236, 1992.

[15] X. Feng, C. White, A. Hajimiri, and M. Roukes, "A self-sustaining ultrahigh-frequency nanoelectromechanical oscillator," *Nature Nanotechnol.*, vol. 3, pp. 342–346, May 2008.

[16] M. Zalalutdinov, K. Aubin, C. Michael, R. B. Reichenbach, T. Alan, A. Zehnder, B. Houston, J. Parpia, and H. Craighead, "Shell-type micromechanical oscillator," presented at the SPIE Int. Symp. Microtechnol. New Millenium, San Agustín, Spain, May 19–21, 2003.

[17] R. Langdon and D. Dowe, "Photoacoustic oscillator sensors," in *Proc. SPIE Conf. Fiber Opt. Sens.*, 1987, pp. 86–93.

[18] K. L. Aubin, M. K. Zalalutdinov, T. Alan, R. B. Reichenbach, R. H. Rand, A. T. Zehnder, J. M. Parpia, and H. G. Craighead, "Limit cycle oscillations in CW laser-driven NEMS," *J. Microelectromech. Syst.*, vol. 13, no. 6, pp. 1018–1026, 2004.

[19] K. Hane and K. Suzuki, "Self-excited vibration of a self-supporting thin film caused by laser irradiation," *Sens. Actuators A, Phys.*, vol. 51, nos. 2–3, pp. 179–182, 1996.

[20] N. Stokes, R. Fatah, and S. Venkatesh, "Self-excited vibrations of optical microresonators," *Electron. Lett.*, vol. 24, no. 13, pp. 777–778, Jun. 1988.

[21] J. David Zook, D. W. Burns, W. R. Herb, H. Guckel, J.-W. Kang, and Y. Ahn, "Optically excited self-resonant microbeams," *Sens. Actuators A, Phys.*, vol. 52, nos. 2–3, pp. 92–98, 1996.

[22] A. Churenkov, "Photothermal excitation and self-excitation of silicon microresonators," *Sens. Actuators A, Phys.*, vol. 39, no. 2, pp. 141–148, 1993.

[23] M. K. Zalalutdinov, A. T. Zehnder, A. Olkhovets, S. W. Turner, L. Sekaric, B. R. Ilic, D. A. Czaplewski, J. M. Parpia, and H. G. Craighead, "Autoparametric optical drive for micromechanical oscillators," *Appl. Phys. Lett.*, vol. 79, no. 5, pp. 695–697, 2001.

[24] S. Lee, M. U. Demirci, and C. T.-C. Nguyen, "A 10-MHz micromechanical resonator pierce reference oscillator for communications," in *11th Int. Conf. Solid-State Sens. Actuators Tech. Dig.*, 2001, pp. 10–14.

[25] L. Lin, R. T. Howe, and A. P. Pisano, "Microelectromechanical filters for signal processing," *J. Microelectromech. Syst.*, vol. 7, no. 3, pp. 286–294, 1998.

[26] S. Kozel, V. Listvin, and A. Churenkov, "Photothermal self-excitation of mechanical microresonators," *Opt. Spectrosc.*, vol. 69, no. 3, pp. 675–677, 1991.

[27] L. Sekaric, M. K. Zalalutdinov, R. B. Bhiladvala, A. T. Zehnder, J. M. Parpia, and H. G. Craighead, "Operation of nanomechanical resonant structures in air," *Appl. Phys. Lett.*, vol. 81, no. 14, pp. 2641–2643, 2002.

[28] C. H. Metzger and K. Karrai, "Cavity cooling of a microlever," *Nature*, vol. 432, pp. 1002–1005, Dec. 2004.

[29] C. H. Metzger, M. Ludwig, C. Neuenhahn, A. Ortlieb, I. Favero, K. Karrai, and F. Marquardt, "Self-induced oscillations in an optomechanical system driven by bolometric backaction," *Phys. Rev. Lett*, vol. 101, no. 13, pp. 133903-1–133903-4, 2008.

[30] T. Kippenberg, H. Rokhsari, T. Carmon, A. Scherer, and K. Vahala, "Analysis of radiation-pressure induced mechanical oscillation of an optical microcavity," *Phys. Rev. Lett.*, vol. 95, no. 3, pp. 033901-1–033901-4, 2005.

[31] H. Rokhsari, T. Kippenberg, T. Carmon, and K. J. Vahala, "Radiation-pressure-driven micro-mechanical oscillator," *Opt. Exp.*, vol. 13, no. 14, pp. 5293–5301, 2005.

[32] O. Arcizet, P. Cohadon, T. Briant, M. Pinard, and A. Heidmann, "Radiation pressure cooling and optomechanical instability of a micromirror," *Nature*, vol. 444, pp. 71–74, Nov. 2006.

[33] S. Gigan, H. Böhm, M. Paternostro, F. Blaser, G. Langer, J. Hertzberg, K. Schwab, D. Bäuerle, M. Aspelmeyer, and A. Zeilinger, "Self-cooling of a micromirror by radiation pressure," *Nature*, vol. 444, pp. 67–70, Nov. 2006.

[34] Q. Lin, J. Rosenberg, X. Jiang, K. J. Vahala, and O. Painter, "Mechanical oscillation and cooling actuated by the optical gradient force," *Phys. Rev. Lett.*, vol. 103, no. 10, pp. 103601-1–103601-4, 2009.

[35] G. Bahl, J. Zehnpfennig, M. Tomes, and T. Carmon, "Stimulated optomechanical excitation of surface acoustic waves in a microdevice," *Nature Commun.*, vol. 2, pp. 1–6, Jul. 2011.

[36] M. W. Pruessner, T. H. Stievater, J. B. Khurgin, and W. S. Rabinovich, "An integrated waveguide-DBR microcavity opto-mechanical system," *Opt. Exp.*, vol. 19, no. 22, pp. 21904–21918, 2011.

[37] D. Rugar and P. Grütter, "Mechanical parametric amplification and theromomechnical noise squeezing," *Phys. Rev. Lett.*, vol. 67, no. 6, pp. 699–702, 1991.

[38] V. Braginsky, S. Strigin, and S. Vyatchanin, "Analysis of parametric oscillatory instability in power recycled LIGO interferometer," *Phys. Lett. A*, vol. 305, nos. 3–4, pp. 111–124, 2002.

[39] C. Hayashi, *Nonlinear Oscillations in Physical Systems*. New York NY, USA: McGraw-Hill, 1964.

[40] A. H. Nayfeh and D. T. Mook, *Nonlinear Oscillations*. Hoboken, NJ, USA: Wiley, 1979.
[41] R. H. Rand, (2012). Lecture Notes on Nonlinear Vibrations, ver. 53 [Online]. Available: http://hdl.handle.net/1813/28989
[42] B. Van der Pol and J. Van der Mark, "Frequency demultiplication," *Nature*, vol. 120, pp. 363–364, Sep. 1927.
[43] B. Van der Pol, "A theory of the amplitude of free and forced triode vibrations," *Radio Rev.*, vol. 1, pp. 701–710, 754–762, 1920.
[44] M. K. Zalalutdinov, K. L. Aubin, M. Pandey, A. T. Zehnder, R. H. Rand, H. G. Craighead, J. M. Parpia, and B. H. Houston, "Frequency entrainment for micromechanical oscillator," *Appl. Phys. Lett.*, vol. 83, no. 16, pp. 3281–3283, 2003.
[45] M. Pandey, K. L. Aubin, M. K. Zalalutdinov, R. B. Reichenbach, A. T. Zehnder, R. H. Rand, and H. G. Craighead, "Analysis of frequency locking in optically driven MEMS resonators," *J. Microelectromech. Syst.*, vol. 15, no. 6, pp. 1546–1554, 2006.
[46] M. Pandey, R. H. Rand, and A. T. Zehnder, "Perturbation analysis of entrainment in a micromechanical limit cycle oscillator," *Commun. Nonlinear Sci. Numer. Simul.*, vol. 12, no. 7, pp. 1291–1301, 2007.
[47] M. Pandey, R. H. Rand, and A. T. Zehnder, "Frequency locking in a forced Mathieu-van der Pol-Duffing system," *Nonlinear Dyn.*, vol. 54, nos. 1–2, pp. 3–12, 2008.
[48] D. Storti and R. H. Rand, "Subharmonic entrainment of a forced relaxation oscillator," *Int. J. Nonlinear Mech.*, vol. 23, no. 3, pp. 231–239, 1988.
[49] K. L. Turner, S. A. Miller, P. G. Hartwell, N. C. MacDonald, S. H. Strogatz, and S. G. Adams, "Five parametric resonances in a microelectromechanical system," *Nature*, vol. 396, pp. 149–152, Nov. 1998.
[50] D. M. Rozelle, "The hemispherical resonator gyroscope: From wineglass to the planets," presented at the AAS/AIAA Spaceflight Mech. Meeting, Savannah, GA, Feb. 8–12 2009.
[51] M. C. Cross, "Improving the frequency precision of oscillators by synchronization," *Phys. Rev. E*, vol. 85, no. 4, pp. 046214-1–046214-8, 2012.
[52] E. Kenig, M. C. Cross, R. Lifshitz, R. Karabalin, L. Villanueva, M. Matheny, and M. Roukes, "Passive phase noise cancellation scheme," *Phys. Rev. Lett.*, vol. 108, no. 26, pp. 264102-1–264102-5, 2012.
[53] M. K. Zalalutdinov, A. Olkhovets, A. T. Zehnder, B. R. Ilic, D. A. Czaplewski, H. G. Craighead, and J. M. Parpia, "Optically pumped parametric amplification for micromechanical oscillators," *Appl. Phys. Lett.*, vol. 78, no. 20, pp. 3142–3144, 2001.
[54] M. A. Hopcroft, W. D. Nix, and T. W. Kenny, "What is the Young's modulus of silicon?" *J. Microelectromech. Syst.*, vol. 19, no. 2, pp. 229–238, 2010.
[55] M. I. Younis, *MEMS Linear and Nonlinear Statics and Dynamics*. Berlin, Germany: Springer, 2011.
[56] J. G. Eisley, "Nonlinear vibration of beams and rectangular plates," *J. Appl. Math. Phys.*, vol. 15, no. 2, pp. 167–175, 1964.
[57] J. G. Eisley, "Large amplitude vibration of buckled beams and rectangular plates," *AIAA J.*, vol. 2, no. 12, pp. 2207–2209, 1964.
[58] D. W. Carr, L. Sekaric, and H. G. Craighead, "Measurement of nanomechanical resonant structures in single crystal silicon," *J. Vac. Sci. Technol. B*, vol. 16, no. 6, pp. 3821–3824, 1998.
[59] D. B. Blocher, "Optically driven limit cycle oscillations in MEMS," Ph.D. dissertation, Dept. Theor. Appl. Mech., Cornell Univ., Ithaca, NY, USA, Aug. 2012.
[60] H. Hu, "Solution of a quadratic nonlinear oscillator by the method of harmonic balance," *J. Sound Vibrat.*, vol. 293, nos. 1–2, pp. 462–468, 2006.
[61] R. Rand, *Topics in Nonlinear Dynamics with Computer Algebra*. New York, NY, USA: Gordon and Breach, 1994.
[62] I. Kozinsky, H. W. C. Postma, I. Bargatin, and M. Roukes, "Tuning nonlinearity, dynamic range, and frequency of nanomechanical resonators," *Appl. Phys. Lett.*, vol. 88, no. 25, pp. 253101-1–253101-3, 2006.

David B. Blocher received the B.S. degree in physics from Duke University, Durham, NC, USA in 2004, and the Ph.D degree in theoretical and applied mechanics from Cornell University, Ithaca, NY, USA in 2012.

He was a Research Scientist at the Lincoln Laboratories, Lexington, MA, USA. He is currently a Post-Doctoral Researcher working on micro-scale atomic combinatorial gyroscopes in the Microsystems Laboratory at the University of California, Irvine, CA, USA. His current research interests include experimental nonlinear vibrations, resonant microelectromechanical systems, and frequency instability in micromechanical devices.

Alan T. Zehnder received the B.S. degree from the University of California, Berkeley, CA, USA, in 1982, and the Ph.D. degree in mechanical engineering with a minor in materials science from the California Institute of Technology, Pasadena, CA, USA, in 1987.

In 1988, he joined the faculty of Cornell University, Ithaca, NY, USA, where he currently serves as an Associate Dean for diversity and faculty development in the Cornell College of Engineering.

Richard H. Rand received the B.S. degree from Cooper Union, New York, NY, USA in 1964, and the M.S. and Sc.D. degrees from Columbia University, New York, NY, USA, in 1965 and 1967, respectively, all in civil engineering.

In 1967, he joined the faculty of Cornell University, Ithaca, NY, USA, where he is currently a member of the Department of Mechanical and Aerospace Engineering and of the Department of Mathematics. He spent sabbatical leaves with the Department of Mechanical Engineering, University of California, Berkeley, in 1982, and the University of California, Los Angeles, in 1989. His current research interests involve using perturbation methods and bifurcation theory to obtain approximate solutions to differential equations arising from nonlinear dynamics problems in engineering and biology.